polysaccharides

MDPI

Article

Impact of the Cross-Linking Agent on the Physicochemical Performance of Alginate Hydrogels and the Release Rate of Immobilized Metronidazole

Anastasia Kuryanova *, Nikolay Glagolev, Vladislav Kaplin, Viktoriya Gorbatova, Yury Gordienko, Nadezhda Aksenova, Alexander Gulin, Victoriya Timofeeva and Anna Solovieva

N. N. Semenov Federal Research Center for Chemical Physics, Russian Academy of Sciences, Moscow 119991, Russia; nikgl@mail.ru (N.G.); piroklas@gmail.com (V.K.); vik21477677@yandex.ru (V.G.); yuagordienko@chph.ras.ru (Y.G.); naksenova@mail.ru (N.A.); vik.timofeeva@gmail.com (V.T.); ann.solovieva@gmail.com (A.S.)

* Correspondence: kuryanovaanastasi@gmail.com

Abstract

In this study, alginate hydrogels (A) cross-linked with a mixture of calcium and europium ions (Ca+Eu)A were developed for the first time as potential carriers for the targeted delivery and sustained release of drugs to specific regions of the gastrointestinal tract. Comparative studies were conducted to investigate the effect of the cross-linking agent (Ca^{2+}, Eu^{3+}, or their mixture) on the physicochemical properties of alginate hydrogels and the release kinetics of metronidazole in media simulating different gastrointestinal environments. Rheological analysis demonstrated that (Ca+Eu)A hydrogels form mechanically robust, highly cross-linked networks. The hydrogels exhibited negligible swelling in an acidic medium (swelling ratio, SR ≈ 1–1.5 g/g); however, in PBS, calcium alginate (CaA) hydrogels swelled 7–8 times more (SR ≈ 42.5 g/g) than hydrogels cross-linked with Eu^{3+} ions or a Ca^{2+}/Eu^{3+} mixture (SR = 5–8 g/g). Metronidazole was released 1.5–2 times faster from calcium-cross-linked hydrogels than from hydrogels cross-linked with Eu^{3+} ions or the mixed Ca^{2+}/Eu^{3+} system, whereas (Ca+Eu)A hydrogels exhibited a more sustained and uniform release profile. These results demonstrate that the drug release kinetics can be tuned by adjusting the Ca^{2+}/Eu^{3+} ratio during alginate cross-linking. Consequently, such hydrogels represent a promising platform for the targeted delivery and controlled release of therapeutic agents, particularly antibiotics, to specific regions of the gastrointestinal tract.

Keywords: alginate hydrogels; Ca^{2+}/Eu^{3+} mixture; rheology; swelling behavior; metronidazole; controlled drug release; gastrointestinal tract

Check for updates

Academic Editors: Tina Maver and Uroš Maver

Received: 6 July 2026
Revised: 4 August 2026
Accepted: 7 August 2026
Published: 13 August 2026
Corrected: 9 November 2026

Copyright: © 2026 by the authors. Licensee MDPI, Basel, Switzerland. This article is an open access article distributed under the terms and conditions of the Creative Commons Attribution (CC BY) license.

1. Introduction

Oral administration is the most common, convenient, and safe method of delivering antibiotics to the human body; however, its efficacy is limited by bioavailability, which is affected by physiological barriers in the gastrointestinal tract, such as fluctuating pH, enzymes, and bile salts [1,2]. In conventional dosage forms, antibiotics are released primarily in the stomach and small intestine, where they are almost completely absorbed. However, the treatment of certain gastrointestinal disorders, including complicated chronic pancreatitis, Crohn's disease, and ulcerative colitis, requires targeted delivery of antibiotics to the

colon [3,4]. Furthermore, the colon represents a potential site for the systemic absorption of various drugs used to treat conditions unrelated to the colon itself [5].

To overcome these limitations, sustained and targeted drug delivery systems based on biopolymers are being actively developed. In particular, biocompatible and biodegradable polysaccharides, such as chitosan, pectin, cellulose, starch, dextran, and alginate (A), are widely used as drug carriers [6–8]. Among these, the anionic polysaccharide sodium alginate (SA) is particularly attractive due to its unique combination of properties, including low immunogenicity, pH sensitivity, and the ability to undergo controlled gelation [9].

Sodium alginate is a linear heteropolymer composed of irregular blocks of β-D-mannuronic acid (M-blocks) and α-L-guluronic acid (G-blocks), and is obtained from brown algae or bacteria of the genera *Azotobacter* and *Pseudomonas* [9,10]. Its high molecular weight (30–600 kDa) enables alginate to undergo gelation in the presence of divalent or trivalent metal cations, forming a three-dimensional polymer network known as a hydrogel. A hydrogel is a network of cross-linked hydrophilic polymer chains capable of retaining large amounts of water (up to 99% of the gel mass) while remaining insoluble [11,12]. This structure facilitates the immobilization of drug substances and their subsequent controlled release in specific regions of the gastrointestinal tract [13,14]. Glutaraldehyde, carbodiimides, and cationic compounds are commonly used to cross-link alginate hydrogels [15–17]. Ionic gelation occurs in the presence of divalent cations (Ca^{2+}, Ba^{2+}, Sr^{2+}, and Zn^{2+}), which form ionic bridges between the carboxyl groups of sodium alginate, giving rise to the well-known "egg-box" model [18–21]. During this process, divalent metal ions bind preferentially to the G-blocks of alginate; consequently, the higher the G-block content of the polymer, the stronger and denser the resulting gel [19,22]. The hydrogel form of alginate is particularly important for oral drug delivery, as it protects the encapsulated drug in the harsh gastric environment by remaining stable and structurally intact, while swelling and gradually releasing the drug in the neutral to alkaline environment of the intestine [23].

The gelation of sodium alginate in the presence of divalent metal salts, particularly calcium chloride ($CaCl_2$), is a rapid and irreversible process that results in the formation of a non-uniformly cross-linked gel, thereby compromising its structural homogeneity [24]. In contrast, alginate-based hydrogels produced via slower gelation exhibit greater structural homogeneity. Calcium salts with low water solubility, such as $CaCO_3$ and $CaSO_4$, dissolve gradually through chemical reactions, leading to a more uniform distribution of Ca^{2+} ions and, consequently, the gradual gelation of alginate hydrogels [25,26].

Trivalent cations can also be used to form three-dimensionally cross-linked alginate hydrogels, although significantly fewer studies have been conducted in this area. Iron (Fe^{3+}) and aluminum (Al^{3+}) ions are the most commonly used cross-linking agents [27–31]. Unlike divalent cations, Fe^{3+} and Al^{3+} do not exhibit block specificity and interact with the carboxylate groups of any uronates (both G and M) along the entire length of the polymer chain.

Alongside the classical ionotropic gelation method, alternative approaches to alginate cross-linking have been actively developed in recent years to overcome the limitations associated with rapid and non-uniform gelation. Among these, bioorthogonal "click" chemistry, particularly strain-promoted azide–alkyne cycloaddition (SPAAC), has emerged as one of the most promising strategies. SPAAC proceeds under physiological conditions without the need for toxic catalysts, thereby ensuring the high biocompatibility of the resulting hydrogels or scaffolds [32]. Another promising approach is photocrosslinking, which involves the preliminary modification of alginate with methacrylate groups followed by photopolymerization in the presence of photoinitiators (e.g., LAP) under UV or visible light. This method enables the rapid in situ formation of covalently cross-linked hydrogels

within seconds, making it particularly attractive for 3D bioprinting and the fabrication of hemostatic materials [33,34]. To further enhance the physicochemical properties of alginate for oral drug delivery, this polysaccharide is often combined with other natural or synthetic polymers, such as gelatin, chitosan, cellulose, pectin, and poly(*N*-isopropylacrylamide) (PNIPAAm). Such composite hydrogels enable the modulation of mucoadhesion, pH responsiveness, and drug release profiles [35–40].

Alginate gels cross-linked with rare-earth element (REE) ions—including europium (Eu^{3+}), terbium (Tb^{3+}), and samarium (Sm^{3+}) [41,42]—are of particular interest for targeted drug delivery systems. These ions possess photoluminescent properties that enable in situ monitoring of drug release in laboratory animals. Specifically, they allow real-time visualization of the carrier's location, monitoring of the drug release rate, and assessment of the uniformity of drug distribution in the intestine. It is important to note that the fluorescence intensity of REE ions depends on their local environment: the leaching of REE ions from the alginate matrix or their complexation with other biomolecules alters both the position of the emission bands and the luminescence intensity. Consequently, these ions can function as integrated optical sensors, including for monitoring carrier degradation. We have previously demonstrated that cross-linking sodium alginate aerogels with REE ions yields highly stable materials [43], further confirming the potential of this approach.

The aim of this study was to develop new types of alginate gels cross-linked with a mixture of divalent and trivalent cations (Ca^{2+}+Eu^{3+}) and to investigate the effect of the cation ratio on the physicochemical properties of these systems. The research objectives included determining how the composition of the cross-linking system influences the stiffness of the cross-linked hydrogels, their degree of swelling, and the release kinetics of metronidazole in model media simulating the acidic environment of the stomach and the neutral environment of the intestine.

Metronidazole (MZ), an antiprotozoal and antimicrobial drug, was used as the model pharmaceutical compound. A previous study [44] demonstrated that hydrogels based on sodium alginate and chitin nanofibers are effective for the controlled release of MZ into various media for the treatment of vaginal infections.

2. Materials and Methods

2.1. Reagents and Preparation of Hydrogels

Sodium alginate (SA) (BioFroxx, Einhausen, Germany; MW 10,000–600,000 g/mol) was dissolved in distilled water to final concentrations of 1 or 2 wt.%. Calcium carbonate ($CaCO_3$) powder (Rushim, analytical grade, Moscow, Russia) and *trans*-2,4-hexadienoic acid (HA) (Shandong Kunda Biotechnology Co., Ltd., Linyi, China) were added to the 1% SA solution, followed by stirring on a magnetic stirrer for 30 min at room temperature. A stable, robustly cross-linked hydrogel was obtained using an SA:$CaCO_3$:HA mass ratio of 1:0.45:0.75. The samples were then left at room temperature for 24 h to allow the sparingly soluble calcium salt to dissolve completely in the alginate solution, resulting in a uniformly cross-linked alginate hydrogel. Finally, the samples were washed with distilled water to remove unreacted calcium ions and sorbic acid.

To obtain alginate hydrogels cross-linked with calcium and europium, calcium alginate (CaA), prepared according to the aforementioned procedure and washed to remove unreacted substances, was immersed in an aqueous solution of europium(III) chloride hexahydrate ($EuCl_3 \cdot 6H_2O$) (Chemkraft, Kaliningrad, Russia) for 24 h. $EuCl_3$ solutions with minimum (0.5%) and maximum (5%) concentrations were used. In addition, CaA hydrogels were treated with a 1% $EuCl_3$ solution, corresponding to an equimolar Ca:Eu ratio in the cross-linking system. The samples were then washed with distilled water to remove excess europium ions.

Europium alginate hydrogel (EuA) was prepared as follows. A 30 mL aliquot of a 2 wt.% $EuCl_3$ solution was poured into a plastic Petri dish containing 15 mL of a 2 wt.% SA solution. The mixture was left to stand for 24 h and then washed with distilled water to remove unreacted europium chloride. The resulting films had a thickness of 1–3 mm and a diameter of 45 mm for the CaA and (Ca+Eu)A hydrogels, and 85 mm for the EuA hydrogel.

The antibiotic metronidazole (MZ) (Metrogyl®, Unique Pharmaceutical Laboratories, Panoli, India) was incorporated into the samples during the film preparation stage. The antibiotic was added to the SA solution together with the cross-linking agents. The MZ concentration in the gels was 1 mg/g.

2.2. Methods for Characterization of Cross-Linked Alginate Gel

2.2.1. Scanning Electron Microscopy

Scanning electron microscopy (SEM) was performed using a Prisma E microscope (Thermo Scientific, Brno, Czech Republic) operated at an accelerating voltage of 5 kV. Thin films were fractured in liquid nitrogen and mounted on L-shaped sample holders. The samples were coated with a 20 nm layer of gold using a Q150R ES Plus sputter coater (Quorum Technologies, Laughton, East Sussex, UK). Secondary electron images were acquired under high-vacuum conditions.

2.2.2. Inductively Coupled Plasma Mass Spectrometry

The concentrations of Na, Ca, and Eu in the samples were determined by inductively coupled plasma mass spectrometry (ICP-MS) following sample pretreatment by acid mineralization. Film samples (6–10 mg) were dissolved in 1 mL of concentrated nitric acid (high-purity grade). Complete dissolution was achieved at 88 °C over 2 h. The resulting solutions were diluted to a final volume of 50 mL with 2% nitric acid in graduated conical polypropylene centrifuge tubes to obtain target element concentrations in the range of 10–100 ppb. Laboratory-grade water (Grade 1 purity according to GOST R 52501-2005) was used for dilution. A control sample preparation procedure was performed concurrently by repeating all the described steps and using the same reagents and materials but omitting the sample. Measurements were performed using a SUPEC 7000 quadrupole mass spectrometer (Focused Photonics Inc., Hangzhou, China) equipped with a dual-pass glass spray chamber cooled to 2 °C, a MicroMist glass nebulizer, and a quartz torch. The instrument operating parameters were optimized prior to analysis. Elemental concentrations in the samples were determined using calibration solutions containing 1, 10, and 100 μg/L of the analytes in 2 vol.% HNO_3. These solutions were prepared by serial dilution of the ICP-MS-A multi-element standard solution (containing Ag, Al, As, B, Ba, Be, Bi, Ca, Ce, Cd, Co, Cr, Cs, Cu, Dy, Er, Eu, Fe, Ga, Gd, Ho, K, In, La, Li, Lu, Mg, Mn, Na, Nb, Nd, Ni, P, Pb, Pr, Re, Rb, Sc, Se, Sr, Sm, Tb, Th, Tl, Tm, U, V, Y, Yb, and Zn), with an analyte concentration of 10 μg/mL.

Based on five replicate measurements, the relative standard deviation of the elemental concentrations in the samples did not exceed 2%.

2.2.3. Atomic Force Microscopy

Atomic force microscopy (AFM) images of the sample surface topography were acquired using a high-spatial-resolution scanning probe microscopy system for surface morphology analysis (NT-MDT LLC, Zelenograd, Moscow, Russia). Etalon probes (NT-MDT, Zelenograd, Moscow, Russia) with a nominal spring constant of 4 N/m, a nominal resonant frequency of 140 kHz, and a nominal tip radius of 10 nm were used. Surface topography was examined in tapping mode, with at least five 10 × 10 μm images for each sample. Image analysis was performed using the Nova software (version SPM 1.2; NT-MDT, Zelenograd, Moscow, Russia).

2.2.4. Spectral Studies

Luminescence spectra of alginate films cross-linked with europium and a calcium–europium mixture were recorded at room temperature using a Horiba Fluoromax Plus spectrofluorometer (Horiba Jobin Yvon, Palaiseau, France). The excitation wavelength was λ_{ex} = 394 nm. The surface chemical structure of the cross-linked alginate films was characterized by attenuated total reflection Fourier transform infrared (ATR-FTIR) spectroscopy using a Spectrum Two spectrometer (PerkinElmer, Shelton, CT, USA) equipped with a high-performance $LiTaO_3$ detector and a standard optical system with KBr windows. Spectra were recorded over the 8300–350 cm^{-1} range at a resolution of 0.5 cm^{-1}. The films were pressed against the surface of the ATR crystal using a flat metal pressure head included in the sample holder assembly.

The release of metronidazole from alginate films into PBS (Eco-Service LLC, Murmansk, Russia; pH 7.2) and 0.1 M HCl (pH 1.2) at 22 °C and 37 °C under constant magnetic stirring was determined by measuring the electronic absorption of metronidazole at λ = 320 nm (extinction coefficient in PBS: ε = 8730 $M^{-1}{\cdot}cm^{-1}$) using a Cary 50 spectrophotometer (Varian, Macquarie Park, NSW, Australia). All experiments were performed in triplicate, and the results are presented as the mean value ± standard deviation.

2.2.5. Rheological Measurements

The rheological properties of the gels were determined using a dynamic shear rheometer (Anton Paar 702e, Graz, Austria) equipped with a parallel-plate geometry (25 mm diameter, 1 mm gap). Samples with a diameter of approximately 25 mm and a height of approximately 1 mm were prepared for analysis. Each sample was placed on the lower plate, and the upper measuring plate was lowered to a gap of 1.1 mm to compress the sample. The sample was then trimmed, if necessary, and the gap was adjusted to the final measurement value of 1 mm. Rheological testing was performed under oscillatory shear at a constant angular frequency (ω) of 10 s^{-1}, with the strain (γ) ranging from 0.001% to 100%. Measurements were carried out at 25 °C and 37 °C. The storage modulus (G′), loss modulus (G″), and complex viscosity (η*) were determined. All measurements were performed in quintuplicate.

2.2.6. Swelling Kinetics of Alginate Hydrogels

The swelling degree of the alginate hydrogels was determined gravimetrically by immersing samples, pre-dried to constant weight and weighed (W_0) using a Sartorius CP1245 analytical balance (Germany), in PBS (pH 7.2) and 0.1 M HCl (pH 1.2) at 22 °C and 37 °C. At predetermined time intervals, the samples were removed from the solutions, excess surface liquid was gently blotted off with filter paper, and the samples were weighed (W_t). Each reported value represents the average of three independent measurements. The swelling degree (SR, g/g) was calculated using the following equation:

$$SR = \frac{W_t - W_0}{W_0}$$

2.2.7. Analysis of Metronidazole Release Kinetics from Cross-Linked Alginate Films

To quantitatively describe the kinetics of MZ release from the hydrogels, the experimental data were fitted using the Higuchi, Korsmeyer–Peppas, and Weibull kinetic models.

All models were applied to the initial stage of drug release, corresponding to ≤60% cumulative drug release. Model parameters were determined by linear regression using the appropriate linearized equations. The goodness of fit was evaluated using the coefficient of determination (R^2). Experiments were performed in triplicate (n = 3), and the data are presented as the mean ± standard deviation (mean ± SD).

2.2.8. Statistical Analysis

All experiments were performed in triplicate (n = 3). Quantitative data are presented as the mean ± standard deviation (SD). Statistical analyses of the hydrogel cross-linking density and antibiotic release parameters were performed using one-way analysis of variance (one-way ANOVA), followed by Tukey's honestly significant difference (HSD) post hoc test for multiple pairwise comparisons. Differences were considered statistically significant at $p < 0.05$. Statistically significant differences in the tables are indicated by superscript letters. Values sharing the same superscript letter within a column are not significantly different ($p > 0.05$), whereas values with different letters differ significantly ($p < 0.05$). Statistical analyses were performed using OriginPro 2018 software (OriginLab Corporation, Northampton, MA, USA).

3. Results and Discussion

3.1. Effect of Crosslinking System Composition on the Metal Content in Gels

As previously mentioned, the fastest method for producing alginate hydrogels cross-linked with Ca^{2+} ions involves the use of an aqueous calcium chloride solution. However, introducing calcium into the alginate solution in this manner results in the formation of a locally gelled, heterogeneous hydrogel with an incompletely cross-linked inner core [45]. This is due to the rapid interaction between Ca^{2+} ions and the carboxyl groups of alginate, with the relaxation time of the slowest stage being on the order of seconds [46]. Various approaches have been proposed to slow the gelation rate and obtain uniformly cross-linked calcium alginate hydrogels, including the use of sparingly soluble calcium salts, the combination of hydrochloric acid with calcium chloride, and freezing of the alginate prior to cross-linking [24,47,48]. In the present study, calcium carbonate ($CaCO_3$) was used as the calcium source. The preparation procedure is described in the Section 2. It is known that when alginate is cross-linked with divalent metal cations, some of the polymer's carboxyl groups remain unreacted [48] and can subsequently interact with europium ions. Europium chloride was therefore used to cross-link these remaining COO^- groups. In this study, hydrogels cross-linked with mixtures of Ca^{2+} and Eu^{3+} ions (Ca+0.5%, 1%, or 5%Eu)A were fabricated. To evaluate the effect of the cross-linking system on gel properties, alginate hydrogels cross-linked exclusively with calcium carbonate (CaA) or europium chloride (EuA) were also prepared. In addition, alginate hydrogels were prepared by simultaneous cross-linking with calcium chloride and europium chloride. However, this approach did not produce a uniformly cross-linked matrix because both Ca^{2+} and Eu^{3+} ions rapidly interact with the carboxyl groups of alginate.

Inductively coupled plasma mass spectrometry (ICP-MS) was used to quantitatively determine the metal ion content in the alginate hydrogels (Table 1). As shown in Table 1, the calcium content in the calcium alginate (CaA) hydrogel was 5.6 wt.%, whereas the europium content in the EuA hydrogel was 17 wt.%. The absence of sodium ions, which were present in the starting polysaccharide, indicates that the gel cross-linking process was complete. However, in fully cross-linked CaA and EuA hydrogels, the theoretical metal contents should be 10 wt.% and 22 wt.%, respectively. In other words, under the experimental conditions, only approximately half of the carboxyl groups in the calcium alginate hydrogel interact with Ca^{2+} ions derived from $CaCO_3$, whereas approximately 77% interact with Eu^{3+} ions. At the same time, the data in Table 1 suggest that in hydrogels cross-linked with both calcium and europium ions, Eu^{3+} interacts primarily with the free carboxyl groups that did not react with $CaCO_3$. This is evidenced by the nearly identical Ca^{2+} content of hydrogels cross-linked with calcium alone and those cross-linked with a mixture of Ca^{2+} and Eu^{3+}. Furthermore, the relatively constant Eu^{3+} content observed in

hydrogels treated with cross-linking systems containing 0.5–5 wt.% of europium supports this conclusion.

Table 1. Elemental composition of cross-linked alginate hydrogels (wt.%) determined by ICP-MS.

Element	Composition (wt.%)				
	CaA *	EuA **	(Ca+0.5%Eu)A	(Ca+1%Eu)A	(Ca+5%Eu)A
Ca	5.6 ± 0.3	-	4.7 ± 0.4	5.1 ± 0.2	5.2 ± 0.4
Eu	-	17.0 ± 0.5	17.2 ± 0.3	17.4 ± 0.4	18.0 ± 0.6

*—theoretical maximum Ca^{2+} content in the alginate hydrogel: 10 wt.%; **—theoretical maximum Eu^{3+} content in the alginate hydrogel: 22 wt.%.

3.2. Microstructure and Surface Structure of Alginate Hydrogels

Figure 1 shows SEM micrographs of the fracture surfaces of alginate hydrogel films cross-linked with Ca^{2+}, Eu^{3+}, and a mixture of both ions. The fracture surface of the Ca^{2+}-cross-linked alginate hydrogel film (CaA) appears largely featureless, except for numerous depressions (Figure 1A). Cross-linking the alginate with Eu^{3+} alone or with a mixture of Ca^{2+} and Eu^{3+} results in a marked change in the hydrogel surface morphology, characterized by the appearance of fine-grained, dense structures (Figures 1B,C and S1). The morphological differences between alginate hydrogels cross-linked with calcium and/or europium ions are evidently attributable to the nature of the cross-linking metal ions. Cross-linking with divalent ions primarily yields a loosely bound "egg-box" structure, whereas the binding of Eu^{3+} to the carboxyl groups of the polysaccharide results in the formation of a dense, three-dimensionally cross-linked network [49].

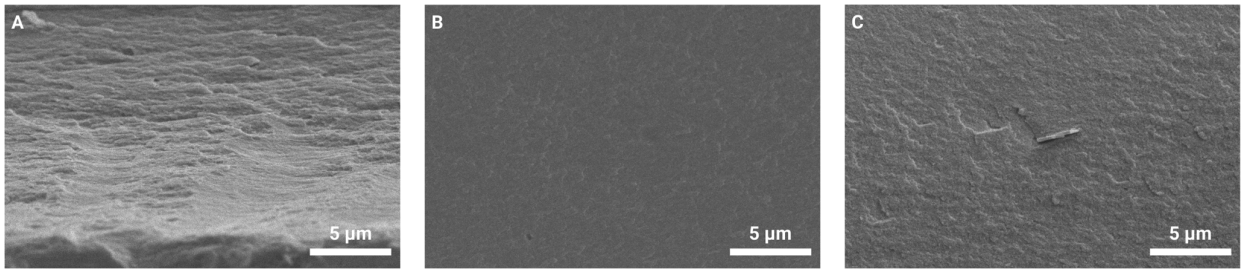


Figure 1. SEM images of fracture surfaces of (**A**) CaA, (**B**) EuA, and (**C**) (Ca+1%Eu) hydrogel films.

These observations are confirmed by AFM analysis of the surfaces of the cross-linked alginate hydrogel films (Figure 2A–C). According to the AFM results, all samples cross-linked with Ca^{2+}, Eu^{3+}, or a mixture of both ions exhibit a granular surface morphology, with grain sizes of approximately 100–140 nm and no distinct structural organization.

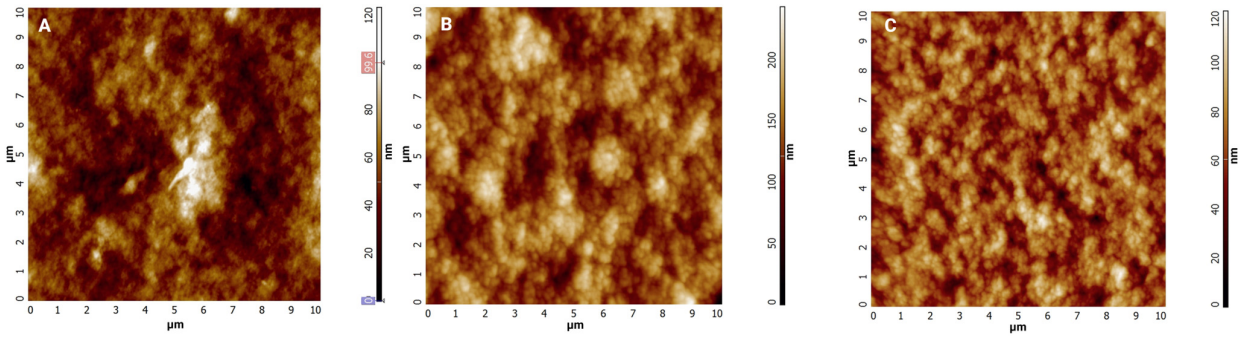


Figure 2. 10 × 10 µm AFM images of the surface topography of (**A**) CaA, (**B**) EuA and (**C**) (Ca+5% Eu)A.

3.3. IR Spectroscopy of Alginate Gels Cross-Linked with Calcium/Europium and a Mixture of Two Metals

The IR spectra of CaA, EuA, and (Ca+Eu)A gels are shown in Figure 3A,B. It should be noted that, in the IR spectra of gels cross-linked with europium or a Ca^{2+}/Eu^{3+} mixture, the absorption band corresponding to the asymmetric stretching vibrations of the carboxylate group is shifted to 1578 cm^{-1} compared with its position at 1590 cm^{-1} in the Ca^{2+}-cross-linked gel (Figure 3A). Similar differences in the IR spectra of such systems have previously been reported [50,51]. According to Hu C. et al. [50], this shift is attributed to differences in the strength of the interaction between the cross-linking cation (calcium or europium) and the carboxylate groups of the alginate macromolecules. A band at 1412 cm^{-1}, corresponding to the symmetric stretching vibrations of COO^- groups, is also observed in the IR spectra of gels cross-linked with calcium, europium, or a mixture of both ions (Figure 3A, curves 1–5). The position and intensity of this band remain essentially unchanged regardless of the cross-linking system. However, in the 3800–2000 cm^{-1} region of the IR spectra, the intensity of the band at 3225 cm^{-1}, assigned to O–H stretching vibrations of the polysaccharide and water, is higher for gels cross-linked with europium or the Ca^{2+}/Eu^{3+} mixture (Figure 3B, curves 2–5). This observation may indicate that cross-linking with europium results in a gel containing a larger number of O–H groups or, more likely, a higher water content. Given that the amount of Eu^{3+} incorporated into the gels is nearly identical in all cases (Table 1) and that europium readily forms coordination complexes with water molecules, the increased intensity of the 3225 cm^{-1} band is most likely associated with water molecules present in the coordination sphere of Eu^{3+} ions.

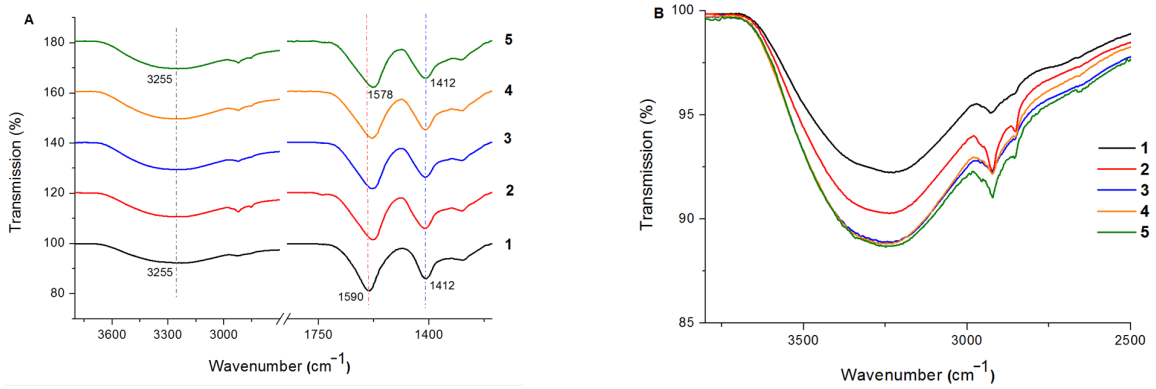


Figure 3. IR spectra (**A**,**B**) of alginate gel cross-linked with (1) calcium, (2) europium, and mixtures (3) (Ca+0.5%Eu)A, (4) (Ca+1%Eu)A, and (5) (Ca+5%Eu)A.

3.4. Investigation of the Photophysical Properties of EuA and (Ca+Eu)A Alginate Hydrogels

It is known that the luminescence spectrum of Eu^{3+} exhibits, among other features, a characteristic emission band at 615 nm, corresponding to the $^5D_0 \rightarrow {}^7F_2$ transition, which is attributed to a hypersensitive electric dipole transition [52]. The intensity of this emission band is strongly influenced by the symmetry of the Eu^{3+} ion's coordination environment, which, in turn, depends on the type and number of chemical bonds formed by the ion [53]. In contrast, the intensity of the $^5D_0 \rightarrow {}^7F_1$ magnetic dipole transition at 591 nm is essentially independent of the local environment and is therefore commonly used as a reference. The asymmetry parameter (ξ), defined as the ratio of the integrated intensities (I) of the hypersensitive (615 nm) and magnetic dipole (591 nm) transitions, provides information about the degree of distortion of the Eu^{3+} ion's coordination sphere and the number of coordination bonds formed [54,55]. In a typical luminescence spectrum of Eu^{3+} salts in aqueous solution, the intensity of the magnetic dipole transition at 591 nm exceeds that of the hypersensitive transition at 615 nm (Figure 4, inset), indicating a highly

symmetric coordination environment resulting from the regular arrangement of water molecules around the ion.

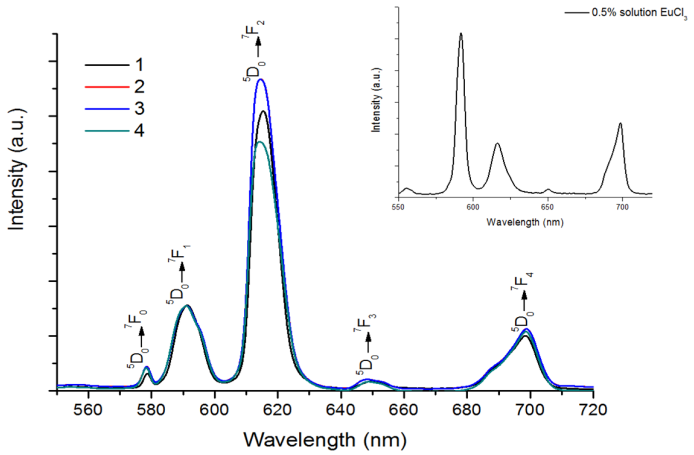


Figure 4. Normalized luminescence spectra of alginate films cross-linked with (1) Eu^{3+} and with Ca^{2+}/Eu^{3+} mixtures: (2) (Ca+0.5%Eu)A, (3) (Ca+1%Eu)A, and (4) (Ca+5%Eu)A. Inset: luminescence spectrum of a 0.5% aqueous $EuCl_3$ solution. Excitation wavelength: λ_{ex} = 394 nm.

Figure 4 shows the luminescence spectra of Eu^{3+} in hydrogels cross-linked with europium and with a mixture of Ca^{2+} and Eu^{3+}. It is evident that, for europium incorporated into the alginate hydrogel matrix, the intensity ratio of the emission bands at 615 nm and 591 nm changes compared with the luminescence spectrum of europium chloride in aqueous solution. The ξ values of the studied samples are presented in Table 2. It is known that, in addition to three ionic interactions with the carboxylate groups of the polymer, each Eu^{3+} ion can form up to 12 additional coordination bonds. In rare-earth element salts, the majority of coordination sites are occupied by water molecules [56]. Upon incorporation of Eu^{3+} ions into the polyanionic alginate matrix, the ξ value increases due to the displacement of water molecules by the larger and less mobile carboxylate groups of alginate macromolecules; this results in a decrease in the symmetry of the Eu^{3+} coordination environment [57]. In the case of secondary cross-linking of Ca^{2+}-containing gels with Eu^{3+} ions, the highest ξ values (3.5–3.6) are observed for samples prepared at low europium concentrations in the cross-linking solutions (0.5% and 1%). This indicates the formation of a highly asymmetric coordination environment around Eu^{3+} ions, associated with a higher effective coordination number. In other words, in alginate initially cross-linked with calcium ions, a sufficient number of free carboxylate groups remain available to participate not only in ionic binding but also in secondary coordination interactions with europium ions. The EuA and (Ca+5%Eu)A samples exhibit lower ξ values (3.25 and 2.9, respectively). These results suggest that, despite similar final Eu^{3+} contents in the cross-linked gels (according to elemental analysis), increasing the concentration of the cross-linking solution leads to Eu^{3+} ions adopting a more symmetric coordination environment. This can be explained from a kinetic perspective: at higher concentrations of rare-earth ions, the diffusion rate increases and cross-linking proceeds more rapidly. Carboxylate groups rapidly coordinate to Eu^{3+} ions via ionic interactions, leading to a sharp decrease in polymer chain mobility, which limits subsequent rearrangement and the formation of additional asymmetric coordination bonds involving water replacement. A more symmetric coordination environment implies denser packing of polymer chains; therefore, increasing the concentration of the cross-linking solution leads to an increase in the density of REE-cross-linked alginate gels.

Table 2. Values of the asymmetry parameter ($\xi = I_{615}/I_{591}$) for alginate films cross-linked with Eu^{3+} ions or a mixture of Ca^{2+} and Eu^{3+} ions.

Sample	ξ
0.5% $EuCl_3$ solution	0.33
EuA	3.2 ± 0.2
(Ca+0.5%Eu)A	3.5 ± 0.1
(Ca+1%Eu)A	3.6 ± 0.1
(Ca+5%Eu)A	2.9 ± 0.3

3.5. Rheological Properties of Cross-Linked Alginate Hydrogels

The efficacy of SA hydrogels for sustained drug release is largely determined by their mechanical and structural properties. Parameters such as the storage modulus (G′), loss modulus (G″), and linear viscoelastic region (LVR) quantitatively characterize the cross-linking density of the polymer network. This density influences both the drug release rate from the matrix and the mechanical stability of the hydrogel, which are crucial for maintaining the integrity of the dosage form until it reaches the target region of the intestine [58]. In this study, the effect of the cross-linking system on the rheological properties of alginate hydrogels was investigated. Figure 5A shows the dependence of the complex viscosity of the hydrogels on strain at 37 °C (measurements performed at room temperature are presented in the Supplementary Information, Figure S2A). At low strain ($\gamma < 0.01\%$), the samples exhibit typical Newtonian behavior with a constant complex viscosity, indicating that the internal gel structure remains intact. A further increase in strain results in a decrease in the complex viscosity of the cross-linked alginate hydrogels, which is attributed to disruption of the polysaccharide network.

The complex viscosity (η*) of gels cross-linked with europium (curve 2) and with mixtures of Ca^{2+} and Eu^{3+} (curves 3–5) is higher than that of the gel cross-linked solely with Ca^{2+} (curve 1). The Ca^{2+}-cross-linked hydrogel exhibits the lowest complex viscosity throughout the investigated strain range and at all test temperatures. The (Ca+Eu)A hydrogels also exhibit an extended linear viscoelastic region (LVR) compared with the Ca^{2+}-cross-linked hydrogel, indicating a stronger cross-linked network. In other words, hydrogels cross-linked with the mixture of cations retain their structural integrity up to higher strain levels than the hydrogel cross-linked with calcium alone.

Figure 5B shows the dependence of the storage modulus (G′) and loss modulus (G″) of the cross-linked alginate hydrogels on strain at 37 °C (data acquired at 25 °C are presented in Figure S2B). The EuA and (Ca+Eu)A hydrogels (curves 2–5) exhibit higher storage modulus (G′) values in the plateau region than the CaA hydrogel (curve 1). The constant G′ value in this region is a direct indicator of the mechanical strength of the hydrogels, reflecting their ability to resist applied deformation. The higher modulus values observed for hydrogels cross-linked with europium or a mixture of cations compared with the calcium alginate hydrogel are attributed to the formation of a more densely cross-linked polymer network [59].

To quantify the expansion of the LVR, its boundary—the critical strain (γ_{cri})—was defined as the strain at which the elastic modulus decreased by 10% from its initial plateau value within the low-strain region. This criterion is commonly used to assess the structural stability of polymer hydrogels [60]. The calculated γ_{cri} values for all samples tested at 22 °C and 37 °C are presented in Table 3. As shown in Table 3, the γ_{cri} values of the (Ca+Eu)A hydrogels are 1.7–4 times higher than those of calcium alginate (CaA) hydrogels at both temperatures. In contrast, hydrogels cross-linked only with europium ions (EuA) exhibit lower γ_{cri} values (0.0031–0.0035%) than (Ca+Eu)A hydrogels (0.0038–0.013%). These

results suggest that dual cross-linking with Ca^{2+} and Eu^{3+} provides an optimal balance between cross-linking density and polymer network flexibility, thereby maximizing the mechanical stability of the hydrogels.

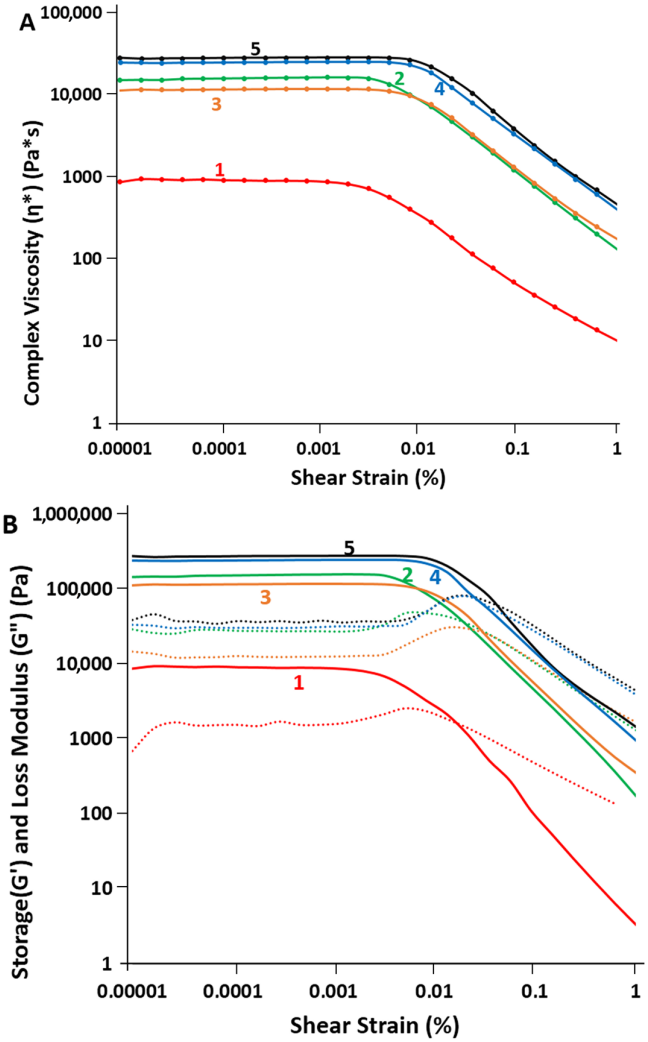


Figure 5. Dependence of the (**A**) complex viscosity, (**B**) storage modulus G′ (solid lines), and loss modulus G″ (dashed lines) of cross-linked alginate hydrogels on strain at 37 °C. Cross-linking systems: (1) CaA, (2) EuA, (3) (Ca+0.5%Eu)A, (4) (Ca+1%Eu)A, and (5) (Ca+5%Eu)A.

Table 3. Strain values of alginate hydrogels at the crossover point (G′ = G″), crossover strain (γ), and critical strain of the linear viscoelastic region (γcri).

Sample	25 °C			37 °C		
	G′ = G″, Pa	γ, %	γcri, %	G′ = G″	γ, %	γcri, %
CaA	12,868 ± 515	0.7 ± 0.3	0.0041 ± 0.0015	1702.5 ± 85	1.6 ± 0.8	0.0017 ± 0.006
EuA	32,189 ± 1247	3.1 ± 0.8	0.0035 ± 0.0018	36,176 ± 1432	2.0 ± 0.5	0.0031 ± 0.0012
(Ca+0.5%Eu)A	26,452 ± 1058	9.9 ± 0.5	0.013 ± 0.0008	26,764 ± 1100	3.0 ± 0.9	0.0038 ± 0.0015
(Ca+1%Eu)A	48,849 ± 1972	10.0 ± 0.7	0.012 ± 0.0010	66,804 ± 2633	2.9 ± 0.3	0.0062 ± 0.0021
(Ca+5%Eu)A	60,210 ± 2399	4.5 ± 0.4	0.0071 ± 0.0022	62,215 ± 2387	4.1 ± 0.6	0.0068 ± 0.0019

The point at which G′ = G″ (the crossover point) corresponds to the transition of the material from a gel-like to a sol-like state. As expected, the crossover point for EuA

and (Ca+Eu)A hydrogels is shifted toward higher strain values compared with that of the calcium-cross-linked alginate hydrogel (Table 3), confirming the greater mechanical strength of hydrogels cross-linked with trivalent europium ions.

The acquired data were used to determine the cross-linking density (ρ_c) of the alginate hydrogels (Table 4) using the following equation:

$$G' = \upsilon RT = 2\rho_c RT$$

where G′ is the storage modulus (Pa), taken as the average G′ value in the plateau region; ν is the concentration of active chains (mol/m^3); ρ_c is the cross-link density (mol/m^3); R is the universal gas constant; and T is the absolute temperature (K).

Table 4. Cross-linking density values of alginate hydrogels as a function of the nature of the cross-linking agent at 25 and 37 °C.

Sample	ρ_c, mol/m^3 (25 °C)	ρ_c, mol/m^3 (37 °C)
CaA	2.7 ± 0.4 ^{a}	1.7 ± 0.25 ^{a}
EuA	31.9 ± 1.6 ^{b}	31 ± 1.4 ^{b}
(Ca+0.5%Eu)A	29.8 ± 2.3 ^{b}	22.7 ± 2.0 ^{c}
(Ca+1%Eu)A	55.4 ± 3.1 ^{c}	48.4 ± 2.9 ^{d}
(Ca+5%Eu)A	59.1 ± 3.6 ^{c}	54.4 ± 2.8 ^{d}

Data are presented as mean ± standard deviation (n = 3). Different superscript letters (a–d) within the same column indicate statistically significant differences between samples (one-way ANOVA, Tukey's post hoc test, $p < 0.05$).

As shown in Table 4, the calcium alginate hydrogel exhibits the lowest cross-link density (1.7–2.7 mol/m^3), corresponding to the lowest stiffness. However, the introduction of as little as 0.5% of europium ions into the cross-linking system leads to a sharp, more than tenfold increase in stiffness (statistically significant, $p < 0.001$), while a europium ion content of 5% increases hydrogel stiffness by approximately 20–30 times. It is important to note that the hydrogel cross-linked solely with Eu^{3+} ions has a cross-link density of 31.9 mol/m^3, which is significantly lower than that of the (Ca+Eu)A samples cross-linked with 1% and 5% Eu^{3+} ($p < 0.01$). This difference is most likely due to the participation of both types of cations in the cross-linking process within the polysaccharide network. Their combined action presumably results in a denser cross-linked structure than that formed using Eu^{3+} ions alone.

According to the designations in Table 4, the following statistical patterns were observed regarding the cross-linking of alginate hydrogels with a mixture of metals. No statistically significant differences in cross-linking density were observed between the (Ca+1%Eu)A and (Ca+5%Eu)A samples at either temperature ($p > 0.05$). This finding suggests that the available carboxyl groups in the alginate network become saturated with Eu^{3+} ions at a europium concentration of 1%, and that increasing the europium content to 5% does not produce any additional cross-linking effect. In contrast, the (Ca+0.5%Eu)A hydrogel exhibited an intermediate cross-linking density, differing significantly from both the (Ca+1%Eu)A and (Ca+5%Eu)A samples ($p < 0.05$).

Table 4 also indicates that the stiffness of the cross-linked gels decreases with increasing temperature. Notably, the cross-link density of calcium alginate hydrogels decreases more significantly than that of hydrogels cross-linked with a mixture of cations; specifically, the cross-link density of Ca-alginate hydrogels decreases by 37% at 37 °C, whereas for gels cross-linked with the (Ca+Eu)A mixture, the decrease in ρ_c is only 8–24%. Moreover, the cross-linking density of EuA remained statistically unchanged upon heating ($p > 0.05$).

This suggests stronger coordination interactions between Eu^{3+} ions and the hydroxyl and carboxyl groups of the polysaccharide compared with Ca^{2+} ions. Thus, incorporation of Eu^{3+} into calcium alginate hydrogels not only increases the cross-link density but also enhances thermal stability, which is a crucial factor for controlled antibiotic release at 37 °C.

3.6. Swelling Kinetics of Cross-Linked Alginate Films in PBS and an Acidic Medium

An important characteristic of drug carriers is their ability to swell in different media, thereby enabling controlled drug release. The swelling ratio (SR), defined as the mass of absorbed fluid per unit mass of dry hydrogel (g/g), was used to quantify the swelling behavior. Figure 6 shows the swelling kinetics of alginate gels cross-linked with Ca^{2+} ions, Eu^{3+} ions, and a mixture of both in phosphate-buffered saline at 22 °C (A) and 37 °C (B); SR is expressed in g/g. Data on the swelling kinetics of the cross-linked alginate hydrogels in 0.1 M hydrochloric acid solution, simulating gastric fluid (SGF), at both temperatures are provided in the Supporting Information. It should be noted that in acidic media, regardless of the cross-linking agent or temperature, the alginate hydrogels exhibit virtually no swelling (Figure S3A,B). This is because, at low pH, carboxylate groups become protonated, leading to the formation of an insoluble alginic acid network [24]. The negligible swelling of cross-linked alginate hydrogels in an acidic environment facilitates the delivery of encapsulated drugs to the intestine while preventing premature release and degradation in the harsh environment of the stomach [61].

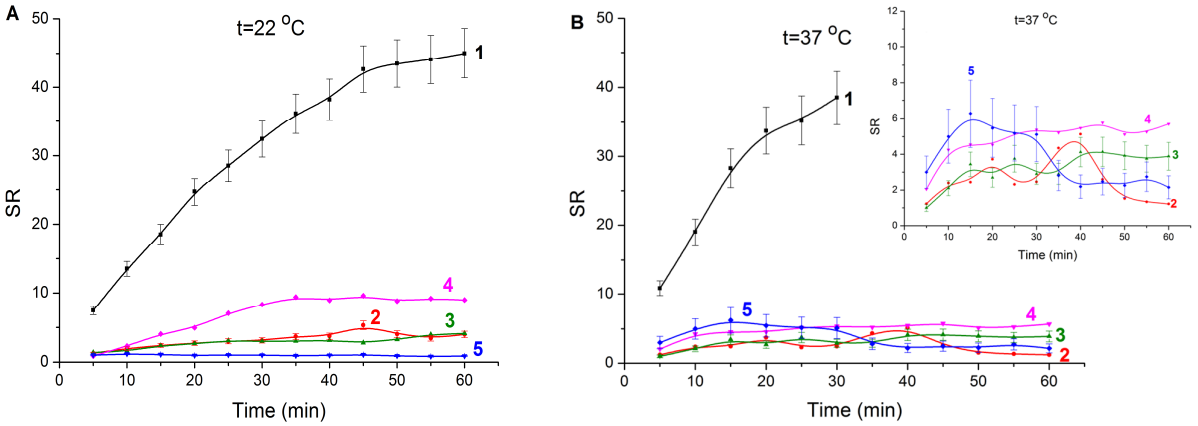


Figure 6. Swelling kinetics of cross-linked alginate hydrogels (1) CaA, (2) EuA, (3) (Ca+0.5% Eu)A, (4) (Ca+1%Eu)A, and (5) (Ca+5%Eu)A in PBS (pH 7.4) at (**A**) t = 22 °C and (**B**) t = 37 °C versus immersion time. The inset in (**B**) shows an enlarged view of the swelling kinetics for samples 2–5 within the 0–12 g/g at t = 37 °C versus immersion time. SR denotes the swelling ratio (g/g), defined as the mass of absorbed PBS per gram of dry hydrogel.

For alginate hydrogels cross-linked only with divalent Ca^{2+} ions, the cross-link density is lower than in systems containing europium ions or mixed Eu^{3+}/Ca^{2+} cross-linking. Accordingly, Ca^{2+}-cross-linked hydrogels exhibit the highest degree of swelling in PBS at both 22 °C and 37 °C compared with hydrogels cross-linked with Eu^{3+} ions or Ca^{2+}/Eu^{3+} mixtures (Figure 6A,B, curves 1–5). Under these conditions, the maximum swelling degree is primarily governed by the type of cross-linking cation and is largely independent of temperature across the studied range (Figure 6A,B, curves 1–5).

It is known that increasing cross-linking density reduces the swelling capacity of hydrogels [62]. Consistent with this, the highest degree of swelling (~40–45 g/g) was observed for calcium-ion-cross-linked hydrogels (Figure 6A,B, curve 1). In contrast, alginate gels cross-linked with europium ions (EuA) or with a combination of Ca^{2+} and Eu^{3+} exhibited significantly lower swelling, not exceeding 2–8 g/g (Figure 6A,B (inset),

curves 2–5). Notably, at 37 °C, the calcium alginate hydrogel loses structural integrity (Figure 6B, curve 1). This is likely due to an ion-exchange process between Na^+ ions from the phosphate-buffered saline and Ca^{2+} ions in the polysaccharide network, which disrupts interchain ionic cross-links $2(\text{-}COO^-)_2\text{-}Ca^{2+}$ within the alginate structure [24]. In contrast, the more densely cross-linked three-dimensional networks of EuA and (Ca+Eu)A hydrogels remain stable over this temperature range. The minor fluctuations in the swelling degree values observed for EuA and (Ca+Eu)A hydrogels (Figure 6B, inset, curves 2–5) throughout the experiment are within the experimental error (n = 3) and are not statistically significant. Therefore, the differences between these samples are considered negligible, and their swelling behavior is discussed collectively. Thus, both the rate and extent of swelling in cross-linked alginate hydrogels are governed primarily by the nature of the cross-linking cation, while the swelling degree is also influenced by the pH of the surrounding medium.

Thus, cross-linking alginate hydrogels with a mixture of Ca^{2+} and Eu^{3+} ions yields a luminescent, highly cross-linked, mechanically robust, and thermally stable carrier that can serve as a matrix for controlled drug delivery. Because dual-metal cross-linking modifies the hydrogels' spectral and mechanical properties, structure, and swelling behavior—factors that may significantly affect antibiotic release—a detailed investigation of the drug release kinetics from the prepared samples is required.

3.7. Kinetics of MZ Release from Cross-Linked Alginate Hydrogels in PBS

As previously noted, (Ca+Eu)A-based hydrogels were developed as carriers for the controlled release of a drug substance (DS) in specific regions of the gastrointestinal tract.

To exclude any influence of the polysaccharide matrix and cross-linking agents on the recorded signal, preliminary spectrophotometric analyses were performed using cross-linked hydrogels without metronidazole. As shown in Figure S4, the UV spectrum of the EuA hydrogel incubated in PBS for 240 min exhibited no absorption bands in the 250–500 nm range (Figure S4, curve 1), where the characteristic absorption band of MZ is located. Similar results were obtained for CaA and (Ca+0.5–5% Eu)A hydrogels. The absence of detectable absorption bands in the spectra of all cross-linked hydrogels confirmed that the calibration curve could be directly applied to determine the concentration of released MZ without correction for the contribution of the alginate matrix.

Furthermore, to confirm the chemical stability of metronidazole under the experimental conditions, an MZ solution was incubated in PBS (pH 7.4) and 0.1 M HCl (pH 1.2) at 37 °C for 240 min, corresponding to the time required for complete MZ release from the hydrogels. As shown in Figure S4, the spectral profiles and absorption maxima remained unchanged throughout the incubation period. The λmax values for MZ were approximately 320 nm in PBS (pH 7.4) (curve 2) and 280 nm in 0.1 M HCl (pH 1.2) (curve 3), which are consistent with previously reported values for native metronidazole [63,64]. The absence of shifts in the absorption maxima or the appearance of new absorption bands indicates that metronidazole does not undergo detectable chemical degradation under the studied conditions.

Thus, the observed increase in the optical density of metronidazole (λmax ≈ 320 nm) during its release from the hydrogels is attributed solely to the increase in MZ concentration in the release medium.

The kinetic release profiles of metronidazole from all investigated cross-linked alginate hydrogels in PBS exhibit a two-stage behavior at both temperatures (22 °C and t = 37 °C) (Figure 7). The temperature of 37 °C was selected to mimic physiological conditions relevant to oral drug delivery, while 22 °C (ambient room temperature) served as a reference condition to evaluate the temperature dependence of the release kinetics. During the first stage (0–15 min), a rapid release of approximately 60–80% of the DS is ob-

served (Table 5). At 37 °C, the release rate from calcium–alginate hydrogels is, as expected, higher than at room temperature: FI increases significantly from 71.8 ± 2.1% at 22 °C to 81.8 ± 1.9% at 37 °C ($p < 0.05$), whereas FII decreases from 28.2 ± 1.8% to 13.0 ± 1.1% ($p < 0.05$). In contrast, cross-linking with europium ions slows the release of metronidazole into the buffer, with only 45–58% released over 15 min. It is worth noting that no statistically significant temperature dependence was observed for any release parameters of the EuA, (Ca+0.5% Eu)A, and (Ca+5% Eu)A samples ($p > 0.05$), confirming the thermal stability of hydrogels cross-linked with Eu^{3+} ions.

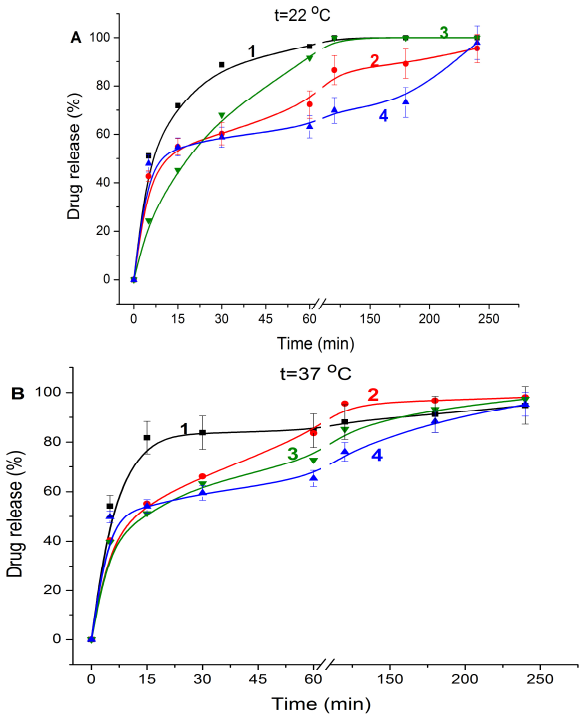


Figure 7. Release kinetics of MZ from cross-linked alginate samples (1) CaA, (2) EuA, (3) (Ca+0.5%Eu)A, and (4) (Ca+5%Eu)A in PBS (pH 7.2) at (**A**) t = 22 °C and (**B**) t = 37 °C.

Table 5. Parameters of the two-stage release of MZ from cross-linked alginate hydrogels in PBS.

Sample	t, °C	F_I, %	F_{II},%	F_{tot},%	ID = F_I/F_{tot}
CaA	22	71.8 ± 2.1 ^{a}	28.2 ± 1.8 ^{a}	100 ^{a}	0.72 ± 0.03 ^{a}
	37	81.8 ± 1.9 ^{b}	13.0 ± 1.1 ^{b}	92.5 ± 1.8 ^{b}	0.86 ± 0.02 ^{b}
EuA	22	54.9 ± 2.3 ^{c}	40.6 ± 2.0 ^{c}	95.5 ± 1.4 ^{c}	0.57 ± 0.02 ^{c}
	37	55.2 ± 2.0 ^{c}	42.9 ± 1.7 ^{c}	98.1 ± 0.8 ^{d}	0.56 ± 0.04 ^{c}
(Ca+0.5%Eu)A	22	45.2 ± 2.4 ^{d}	54.8 ± 2.2 ^{d}	100 ^{a}	0.45 ± 0.03 ^{d}
	37	45.1 ± 2.5 ^{d}	52.3 ± 1.6 ^{d}	97.4 ± 2.2 ^{ac}	0.46 ± 0.04 ^{d}
(Ca+5%Eu)A	22	54.8 ± 2.2 ^{c}	43.1 ± 2.1 ^{c}	97.9 ± 0.5 ^{cd}	0.56 ± 0.03 ^{c}
	37	54.1 ± 2.2 ^{c}	41.1 ± 1.9 ^{c}	95.2 ± 1.5 ^{c}	0.57 ± 0.02 ^{c}

F_I (%)—fraction of DS released from the sample during stage I (15 min); F_{II} (%)—fraction of DS released from the sample during stage II (225 min); F_{tot} (%)—fraction of DS released from the sample over 240 min; Data are presented as mean ± standard deviation (n = 3). Different superscript letters (a–d) within the same column indicate statistically significant differences between samples (one-way ANOVA, Tukey's post hoc test, $p < 0.05$).

During the second stage (15–240 min), a pronounced slowdown in the drug release rate was observed; notably, increasing the europium content in the gel markedly reduced

the release rate. Specifically, at 22 °C, 100% of MZ was released from CaA and (Ca+0.5% Eu)A gels by 120 min, whereas EuA and (Ca+5% Eu)A gels released only approximately 97% by 240 min. Over the subsequent 225 min at 37 °C, 13.0% of MZ was released from CaA hydrogels, while in alginate gels cross-linked with Eu^{3+} or with a combination of Ca^{2+} and Eu^{3+}, the release rate decreased by a factor of 2 to 3.3 (Figure 7B, Table 5). To provide a quantitative description, a two-stage index (ID = F_I/F_{tot}) was calculated, representing the fraction of antibiotic released during the initial stage relative to the total release of DS over the entire period. Cross-linking CaA hydrogels with europium slows DS release during the first stage, thereby increasing the relative contribution of the second stage. The most uniform release profile was observed for EuA and (Ca+5%Eu)A samples (ID = 0.56–0.57) at both temperatures, with no statistically significant differences found between these samples ($p > 0.05$). The highest ID value (0.86) was recorded for the CaA hydrogel at 37 °C, indicating a dominance of the rapid-release phase.

It is important to note that in an acidic medium, metronidazole was not released from the studied samples at either room temperature or elevated temperature (37 °C).

Three kinetic models were applied to quantitatively analyze the antibiotic release kinetics from cross-linked alginate gels.

The Higuchi model (Equation (1)) was used to describe the initial diffusion-controlled release of DS from the polymer matrix (up to 60% release):

$$\frac{M_t}{M_\infty} = K_H\sqrt{t} \quad (1)$$

where M_t is the amount of drug released at time t(g), M_∞ is the total amount of antibiotic in the film (g), and K_H is the Higuchi release rate constant ($min^{-1/2}$).

The Korsmeyer–Peppas model (Equation (2)) was applied to provide a more detailed description of the drug release mechanism.

$$\frac{M_t}{M_\infty} = K * t^n \quad (2)$$

where K is the rate constant and n is the release exponent characterizing the DS release mechanism. Specifically, $n \leq 0.5$ corresponds to Fickian diffusion, $0.5 < n < 1$ indicates anomalous (non-Fickian) transport associated with both diffusion and polymer chain relaxation or swelling, and $n = 1$ reflects transport, typically governed by zero-order kinetics due to polymer erosion or swelling-controlled release.

This model accounts for both Fickian and non-Fickian release mechanisms in swelling and non-swelling systems; however, its applicability is generally limited to the initial stage of release (up to approximately 60% of the total drug release).

The Weibull model (Equation (3)) was used to describe the entire release profile, including the initial burst release followed by a subsequent slowdown.

$$\frac{M_t}{M_\infty} = 1 - e^{\left(\frac{t}{\tau}\right)^\beta} \quad (3)$$

τ is the scale parameter (the time corresponding to the release of approximately 63.2% of DS, min), and β is the shape parameter characterizing the release mechanism. Specifically, $\beta < 1$ indicates a rapid initial release followed by deceleration, $\beta = 1$ corresponds to exponential kinetics, and $\beta > 1$ describes a sigmoidal release profile with an initial lag phase followed by accelerated release.

These models enable characterization of both the initial burst release and the prolonged diffusion stage, which is particularly important for comparative analysis of hydrogels with different cross-linking densities [65]. Table 6 shows that the models confirm

the fastest antibiotic release occurred in PBS from calcium–alginate hydrogels at 37 °C (Table S1—t = 22 °C). This is reflected in the highest K_H values and the largest rate constants in the Korsmeyer–Peppas model, as well as the lowest n and β values. The minimum time required for release of 63% of the antibiotic from the gels was τ = 5.58 min. The Korsmeyer–Peppas model allowed assessment of the release mechanism based on the exponent n. For all samples, n < 0.45, corresponding to Fickian diffusion, indicating that drug release was governed predominantly by diffusion. Cross-linking calcium–alginate hydrogels with Eu^{3+} ions slowed the initial drug release rate by a factor of 1.25–1.8 according to the Higuchi and Korsmeyer–Peppas models. The Weibull model indicates a more gradual and controlled release in samples cross-linked with rare-earth ions or Ca^{2+}/Eu^{3+} mixtures; specifically, the time required to release 63% of the antibiotic increases by a factor of 1.5–4.7. Thus, cross-linking density is a key determinant of release kinetics. The denser polymer networks formed in alginate hydrogels cross-linked with europium or Ca^{2+}/Eu^{3+} mixtures reduce antibiotic diffusion, an effect quantitatively described by the parameters of the Higuchi, Korsmeyer–Peppas, and Weibull models.

Table 6. Correlation coefficients and kinetic parameters of mathematical models describing MZ release from alginate hydrogels in PBS at 37 °C.

Sample	Higuchi Model	Korsmeyer–Peppas Model			Weibull Model		
	K_H, $min^{-1/2}$	K	n	R^2	β	τ, min	R^2
CaA	0.226	0.519	0.116	0.955	0.278	5.58	0.963
EuA	0.164	0.289	0.238	0.989	0.539	18.54	0.997
(Ca+0.5% Eu)A	0.159	0.357	0.187	0.968	0.423	17.53	0.979
(Ca+5% Eu)A	0.181	0.330	0.170	0.941	0.363	26.3	0.998

4. Conclusions

This study investigated the effect of the nature of the cross-linking agent on the physicochemical properties of alginate hydrogels and the release kinetics of metronidazole from these carriers in PBS. It was demonstrated that cross-linking alginate with a mixture of Ca^{2+} and Eu^{3+} ions modifies the structural, rheological, and swelling properties of the hydrogels compared with calcium alginate (CaA). Ionic and coordination interactions between Eu^{3+} ions and the carboxylate and hydroxyl groups of alginate chains in (Ca+Eu)A hydrogels promote the formation of a densely cross-linked three-dimensional network, imparting enhanced mechanical strength, resistance to deformation at 22 and 37 °C, and luminescent properties. The study also showed that, in an acidic medium, all hydrogels exhibited negligible swelling (swelling ratio of approximately 1–1.5 g/g), whereas in PBS (pH 7.2), CaA hydrogels swelled significantly more than those cross-linked with Eu^{3+} ions or a Ca^{2+}/Eu^{3+} mixture. In vitro metronidazole release studies demonstrated that the (Ca+5% Eu)A hydrogel exhibited the most uniform antibiotic release profile in PBS at both 22 and 37 °C. Furthermore, varying the Ca^{2+}/Eu^{3+} ratio in the cross-linking system enabled modulation of both the release rate and the duration of drug release. Overall, these findings demonstrate that (Ca+Eu)A hydrogels represent a promising platform for the controlled and targeted delivery of drugs to specific regions of the gastrointestinal tract.

Supplementary Materials: The following supporting information can be downloaded at https://www.mdpi.com/article/10.3390/polysaccharides7030096/s1, Figure S1: SEM images of fracture surfaces of (A) (Ca+0.5%Eu)A, (B) (Ca+5%Eu)A hydrogel films; Figure S2: Dependence of the (A) complex viscosity, (B) storage modulus G′ (solid lines), and loss modulus G″ (dashed lines) of cross-linked alginate hydrogels on strain at 25 °C. Cross-linking systems: (1) CaA, (2) EuA,

(3) (Ca+0.5% Eu)A, (4) (Ca+1%Eu)A, and (5) (Ca+5%Eu)A; Figure S3: Swelling kinetics of cross-linked alginate hydrogels (1) CaA, (2) EuA, (3) (Ca+0.5%Eu)A, (4) (Ca+1%Eu)A, and (5) (Ca+5%Eu)A in 0.1 M HCl (pH 1.2) at (A) t = 22 °C and (B) t = 37 °C versus immersion time; Figure S4: Electronic absorption spectra of EuA hydrogel in PBS (1), MTZ solution in PBS (2), MTZ solution in 0.1 M HCl (3), and EuA hydrogel containing MTZ in PBS (4). All samples were incubated in PBS at 37 °C for 240 min; Table S1: Correlation coefficients and kinetic parameters of mathematical models describing MTZ release from alginate hydrogels in PBS at 22 °C.

Author Contributions: Conceptualization, A.K. and A.S.; methodology, A.K. and N.G.; investigation, A.K., N.G., V.G., A.G., N.A., Y.G. and V.T.; resources, Y.G., A.G., V.K. and V.G.; data curation, A.S.; writing—original draft preparation, A.K.; writing—review and editing, A.K., N.A., V.K. and A.S.; visualization, A.K., A.G., V.K., V.G. and V.T.; supervision, A.S. All authors have read and agreed to the published version of the manuscript.

Funding: This study was supported by the Russian Science Foundation (grant No. 25-23-00989).

Data Availability Statement: The original contributions presented in this study are included in the article/Supplementary Material. Further inquiries can be directed to the corresponding author.

Conflicts of Interest: The authors declare no conflicts of interest.

References

1. Homayun, B.; Lin, X.; Choi, H.-J. Challenges and Recent Progress in Oral Drug Delivery Systems for Biopharmaceuticals. *Pharmaceutics* **2019**, *11*, 129. [CrossRef]
2. Raza, A.; Sime, F.B.; Cabot, P.J.; Maqbool, F.; Roberts, J.A.; Falconer, J.R. Solid Nanoparticles for Oral Antimicrobial Drug Delivery: A Review. *Drug Discov. Today* **2019**, *24*, 858–866. [CrossRef]
3. Amidon, S.; Brown, J.E.; Dave, V.S. Colon-Targeted Oral Drug Delivery Systems: Design Trends and Approaches. *AAPS PharmSciTech* **2015**, *16*, 731–741. [CrossRef] [PubMed]
4. Belali, N.; Wathoni, N.; Muchtaridi, M. Advances in Orally Targeted Drug Delivery to Colon. *J. Adv. Pharm. Technol. Res.* **2019**, *10*, 100–106. [CrossRef] [PubMed]
5. Lou, J.; Duan, H.; Qin, Q.; Teng, Z.; Gan, F.; Zhou, X.; Zhou, X. Advances in Oral Drug Delivery Systems: Challenges and Opportunities. *Pharmaceutics* **2023**, *15*, 484. [CrossRef] [PubMed]
6. Miao, T.; Wang, J.; Zeng, Y.; Liu, G.; Chen, X. Polysaccharide-Based Controlled Release Systems for Therapeutics Delivery and Tissue Engineering: From Bench to Bedside. *Adv. Sci.* **2018**, *5*, 1700513. [CrossRef] [PubMed]
7. Azehaf, H.; Benzine, Y.; Tagzirt, M.; Skiba, M.; Karrout, Y. Microbiota-Sensitive Drug Delivery Systems Based on Natural Polysaccharides for Colon Targeting. *Drug Discov. Today* **2023**, *28*, 103606. [CrossRef] [PubMed]
8. Tie, S.; Tan, M. Current Advances in Multifunctional Nanocarriers Based on Marine Polysaccharides for Colon Delivery of Food Polyphenols. *J. Agric. Food Chem.* **2022**, *70*, 903–915. [CrossRef] [PubMed]
9. Sanchez-Ballester, N.M.; Bataille, B.; Soulairol, I. Sodium Alginate and Alginic Acid as Pharmaceutical Excipients for Tablet Formulation: Structure-Function Relationship. *Carbohydr. Polym.* **2021**, *270*, 118399. [CrossRef] [PubMed]
10. Hariyadi, D.M.; Islam, N. Current Status of Alginate in Drug Delivery. *Adv. Pharmacol. Pharm. Sci.* **2020**, *2020*, 8886095. [CrossRef] [PubMed]
11. Román-Guerrero, A.; Cortés-Camargo, S.; Alpizar-Reyes, E.; Fabela-Morón, M.F.; Cruz-Olivares, J.; Velázquez-Gutiérrez, S.K.; Pérez-Alonso, C. Chemically Modified Alginate-Based Hydrogel-Matrices in Drug Delivery. *Macromol* **2025**, *5*, 36. [CrossRef]
12. Zhu, T.; Mao, J.; Cheng, Y.; Liu, H.; Lv, L.; Ge, M.; Li, S.; Huang, J.; Chen, Z.; Li, H.; et al. Recent Progress of Polysaccharide-Based Hydrogel Interfaces for Wound Healing and Tissue Engineering. *Adv. Mater. Interfaces* **2019**, *6*, 1900761. [CrossRef]
13. Zou, Z.; Zhang, B.; Nie, X.; Cheng, Y.; Hu, Z.; Liao, M.; Li, S. A Sodium Alginate-Based Sustained-Release IPN Hydrogel and Its Applications. *RSC Adv.* **2020**, *10*, 39722–39730. [CrossRef] [PubMed]
14. Sharpe, L.A.; Daily, A.M.; Horava, S.D.; Peppas, N.A. Therapeutic Applications of Hydrogels in Oral Drug Delivery. *Expert Opin. Drug Deliv.* **2014**, *11*, 901–915. [CrossRef] [PubMed]
15. Kulkarni, A.R.; Soppimath, K.S.; Aminabhavi, T.M.; Dave, A.M.; Mehta, M.H. Glutaraldehyde Crosslinked Sodium Alginate Beads Containing Liquid Pesticide for Soil Application. *J. Control. Release* **2000**, *63*, 97–105. [CrossRef] [PubMed]
16. Milivojević, M.; Popović, A.; Pajić-Lijaković, I.; Šoštarić, I.; Kolašinac, S.; Stevanović, Z.D. Alginate Gel-Based Carriers for Encapsulation of Carotenoids: On Challenges and Applications. *Gels* **2023**, *9*, 620. [CrossRef] [PubMed]
17. Ručigaj, A.; Golobič, J.; Kopač, T. The Role of Multivalent Cations in Determining the Cross-Linking Affinity of Alginate Hydrogels: A Combined Experimental and Modeling Study. *Chem. Eng. J. Adv.* **2024**, *20*, 100678. [CrossRef]

18. Wang, Y.; Shen, Z.; Wang, H.; Song, Z.; Yu, D.; Li, G.; Liu, X.; Liu, W. Progress in Research on Metal Ion Crosslinking Alginate-Based Gels. *Gels* **2024**, *11*, 16. [CrossRef] [PubMed]
19. Makarova, A.O.; Derkach, S.R.; Khair, T.; Kazantseva, M.A.; Zuev, Y.F.; Zueva, O.S. Ion-Induced Polysaccharide Gelation: Peculiarities of Alginate Egg-Box Association with Different Divalent Cations. *Polymers* **2023**, *15*, 1243. [CrossRef] [PubMed]
20. Larsen, B.E.; Bjørnstad, J.; Pettersen, E.O.; Tønnesen, H.H.; Melvik, J.E. Rheological Characterization of an Injectable Alginate Gel System. *BMC Biotechnol.* **2015**, *15*, 29. [CrossRef] [PubMed]
21. Tordi, P.; Ridi, F.; Samorì, P.; Bonini, M. Cation-Alginate Complexes and Their Hydrogels: A Powerful Toolkit for the Development of Next-Generation Sustainable Functional Materials. *Adv. Funct. Mater.* **2025**, *35*, 2416390. [CrossRef]
22. Song, H.-L.; Wang, Y.-Q.; Zhang, Q.; Liu, Y.; Zhang, L.-D.; Yan, J.-N.; Lai, B.; Wang, C.; Wu, H.-T. Improvement of Gel Properties of Low-Salt Shrimp (Litopenaeus Vannamei) Surimi by Sodium Alginate: Effect of Mannuronic Acid/Guluronic Acid Ratios. *Int. J. Biol. Macromol.* **2025**, *330*, 148037. [CrossRef] [PubMed]
23. Foroutan, R.; Mohammadzadeh, A.; Javanbakht, S.; Mohammadi, R.; Ghorbani, M. Alginate/Magnetic Hydroxyapatite Bio-Nanocomposite Hydrogel Bead as a pH-Responsive Oral Drug Carrier for Potential Colon Cancer Therapy. *Results Chem.* **2025**, *15*, 102177. [CrossRef]
24. Malektaj, H.; Drozdov, A.D.; deClaville Christiansen, J. Swelling of Homogeneous Alginate Gels with Multi-Stimuli Sensitivity. *Int. J. Mol. Sci.* **2023**, *24*, 5064. [CrossRef] [PubMed]
25. Lin, X.; Shi, J.; Meng, G.; Yu, C. Sodium Alginate Hydrogel Carrier with Calcium Carbonate as Calcium Source for Ibuprofen Release. *Macromol. Chem. Phys.* **2023**, *224*, 2300195. [CrossRef]
26. Satriaji, K.P.; Garcia, C.V.; Kim, G.H.; Shin, G.H.; Kim, J.T. Antibacterial Bionanocomposite Films Based on CaSO4-Crosslinked Alginate and Zinc Oxide Nanoparticles. *Food Packag. Shelf Life* **2020**, *24*, 100510. [CrossRef]
27. Massana Roquero, D.; Othman, A.; Melman, A.; Katz, E. Iron(III)-Cross-Linked Alginate Hydrogels: A Critical Review. *Mater. Adv.* **2022**, *3*, 1849–1873. [CrossRef]
28. Narayanan, R.P.; Melman, G.; Letourneau, N.J.; Mendelson, N.L.; Melman, A. Photodegradable Iron(III) Cross-Linked Alginate Gels. *Biomacromolecules* **2012**, *13*, 2465–2471. [CrossRef] [PubMed]
29. Nokhodchi, A.; Tailor, A. In Situ Cross-Linking of Sodium Alginate with Calcium and Aluminum Ions to Sustain the Release of Theophylline from Polymeric Matrices. *IL Farm.* **2004**, *59*, 999–1004. [CrossRef] [PubMed]
30. Urbanova, M.; Pavelkova, M.; Czernek, J.; Kubova, K.; Vyslouzil, J.; Pechova, A.; Molinkova, D.; Vyslouzil, J.; Vetchy, D.; Brus, J. Interaction Pathways and Structure–Chemical Transformations of Alginate Gels in Physiological Environments. *Biomacromolecules* **2019**, *20*, 4158–4170. [CrossRef] [PubMed]
31. Sterner, M.; Edlund, U. High-Performance Filaments from Fractionated Alginate by Polyvalent Cross-Linking: A Theoretical and Practical Approach. *Biomacromolecules* **2018**, *19*, 3311–3330. [CrossRef] [PubMed]
32. Buwalda, S.J. 'Click' Hydrogels from Renewable Polysaccharide Resources: Bioorthogonal Chemistry for the Preparation of Alginate, Cellulose and Other Plant-Based Networks with Biomedical Applications. *Int. J. Biol. Macromol.* **2024**, *282*, 136695. [CrossRef] [PubMed]
33. Liu, Y.; Zhang, Y.; Jia, Q.; Liang, X.; Xu, K. Rapid in Situ Formation of a Double Cross-Linked Network Hydrogels for Wound Healing Promotion. *Front. Pharmacol.* **2025**, *16*, 1562264. [CrossRef] [PubMed]
34. Zhang, M.; Hou, L.; Song, W.; Tan, Y.; Huang, Y.; Li, Z.; Huang, X.; Kong, Y.; Zhang, C.; Liang, L.; et al. Development of an Alginate-Based Bioink with Enhanced Hemostatic and Antibacterial Properties. *Int. J. Biol. Macromol.* **2025**, *302*, 140549. [CrossRef] [PubMed]
35. Elsayed, E.W.; El-Ashmawy, A.A.; El-Bassyouni, G.T.; Mousa, S.M.; El-Manawaty, M.; Emara, L.H. Formulation and Evaluation of Alginate-Gelatin Hydrogel Scaffolds Loaded with Zinc-Doped Hydroxyapatite and 5-Fluorouracil. *Int. J. Biol. Macromol.* **2023**, *237*, 124147. [CrossRef] [PubMed]
36. Unagolla, J.M.; Jayasuriya, A.C. Drug Transport Mechanisms and in Vitro Release Kinetics of Vancomycin Encapsulated Chitosan-Alginate Polyelectrolyte Microparticles as a Controlled Drug Delivery System. *Eur. J. Pharm. Sci.* **2018**, *114*, 199–209. [CrossRef] [PubMed]
37. Lin, N.; Gèze, A.; Wouessidjewe, D.; Huang, J.; Dufresne, A. Biocompatible Double-Membrane Hydrogels from Cationic Cellulose Nanocrystals and Anionic Alginate as Complexing Drugs Codelivery. *ACS Appl. Mater. Interfaces* **2016**, *8*, 6880–6889. [CrossRef] [PubMed]
38. Szekalska, M.; Czajkowska-Kośnik, A.; Maciejewski, B.; Misztalewska-Turkowicz, I.; Wilczewska, A.Z.; Bernatoniene, J.; Winnicka, K. Mucoadhesive Alginate/Pectin Films Crosslinked by Calcium Carbonate as Carriers of a Model Antifungal Drug—Posaconazole. *Pharmaceutics* **2023**, *15*, 2415. [CrossRef] [PubMed]
39. Liu, Y.-Q.; Guo, H.-Y.; Hu, C.-Y.; Xu, X. A Novel Dual PH- and Temperature-Responsive Poly (N-Isopropylacrylamide)/Polyacrylamide/Calcium Alginate Hydrogel with Robust Mechanical Performance and Biocompatibility for Sustainable Drug Release. *Polymer* **2025**, *327*, 128386. [CrossRef]

40. Tomić, S.L.; Babić Radić, M.M.; Vuković, J.S.; Filipović, V.V.; Nikodinovic-Runic, J.; Vukomanović, M. Alginate-Based Hydrogels and Scaffolds for Biomedical Applications. *Mar. Drugs* **2023**, *21*, 177. [CrossRef] [PubMed]
41. Wu, S.-Y.; An, Y.-N.; Yeh, Y.-C. Lanthanide Ionic Radius Modulation for Tailored Triple-Cross-Linked Luminescent Gelatin/Alginate Hydrogels: Structural, Mechanical, and Sensing Insights. *JACS Au* **2025**, *5*, 4022–4035. [CrossRef] [PubMed]
42. Freire, R.V.M.; Coelho, D.M.A.; Maciel, L.G.; Jesus, L.T.; Freire, R.O.; Dos Anjos, J.V.; Junior, S.A. Luminescent Supramolecular Metallogels: Drug Loading and Eu(III) as Structural Probe. *Chem. A Eur. J.* **2024**, *30*, e202400680. [CrossRef] [PubMed]
43. Kaplin, V.; Kopylov, A.; Koryakovtseva, A.; Minaev, N.; Epifanov, E.; Gulin, A.; Aksenova, N.; Timashev, P.; Kuryanova, A.; Shershnev, I.; et al. Features of Luminescent Properties of Alginate Aerogels with Rare Earth Elements as Photoactive Cross-Linking Agents. *Gels* **2022**, *8*, 617. [CrossRef] [PubMed]
44. Dubashynskaya, N.V.; Petrova, V.A.; Romanov, D.P.; Skorik, Y.A. pH-Sensitive Drug Delivery System Based on Chitin Nanowhiskers–Sodium Alginate Polyelectrolyte Complex. *Materials* **2022**, *15*, 5860. [CrossRef] [PubMed]
45. Hu, C.; Lu, W.; Mata, A.; Nishinari, K.; Fang, Y. Ions-Induced Gelation of Alginate: Mechanisms and Applications. *Int. J. Biol. Macromol.* **2021**, *177*, 578–588. [CrossRef] [PubMed]
46. Kuo, C.K.; Ma, P.X. Ionically Crosslinked Alginate Hydrogels as Scaffolds for Tissue Engineering: Part 1. Structure, Gelation Rate and Mechanical Properties. *Biomaterials* **2001**, *22*, 511–521. [CrossRef] [PubMed]
47. Warburton, L.; Rubinsky, B. Freezing-Modulated-Crosslinking: A Crosslinking Approach for 3D Cryoprinting. *Bioprinting* **2022**, *27*, e00225. [CrossRef]
48. Zhang, Q.; Yan, Y.; Li, Z.; Du, J.; Zhang, K.; Zhang, L.; Wang, T.; Bianco, A.; Ge, S.; Ma, B. A Uniform-Unsaturated Crosslinking Strategy to Construct Injectable Alginate Hydrogel. *Int. J. Biol. Macromol.* **2024**, *254*, 127726. [CrossRef] [PubMed]
49. Choi, I.; Lee, Y.; Lyu, J.S.; Lee, J.-S.; Han, J. Characterization of Ionically Crosslinked Alginate Films: Effect of Different Anion-Based Metal Cations on the Improvement of Water-Resistant Properties. *Food Hydrocoll.* **2022**, *131*, 107785. [CrossRef]
50. Hu, C.; Wang, M.X.; Sun, L.; Yang, J.H.; Zrínyi, M.; Chen, Y.M. Dual-Physical Cross-Linked Tough and Photoluminescent Hydrogels with Good Biocompatibility and Antibacterial Activity. *Macromol. Rapid Commun.* **2017**, *38*, 1600788. [CrossRef] [PubMed]
51. Papageorgiou, S.K.; Kouvelos, E.P.; Favvas, E.P.; Sapalidis, A.A.; Romanos, G.E.; Katsaros, F.K. Metal–Carboxylate Interactions in Metal–Alginate Complexes Studied with FTIR Spectroscopy. *Carbohydr. Res.* **2010**, *345*, 469–473. [CrossRef] [PubMed]
52. Ma, Q.; Wang, Q. Lanthanide Induced Formation of Novel Luminescent Alginate Hydrogels and Detection Features. *Carbohydr. Polym.* **2015**, *133*, 19–23. [CrossRef] [PubMed]
53. Thor, W.; Carneiro Neto, A.N.; Moura, R.T.; Wong, K.-L.; Tanner, P.A. Europium(III) Coordination Chemistry: Structure, Spectra and Hypersensitivity. *Coord. Chem. Rev.* **2024**, *517*, 215927. [CrossRef]
54. Chiu, T.-H.; Wu, S.-Y.; Yang, Y.-C.; Yan, C.-J.; Yeh, Y.-C. Fabrication of Luminescent Triple-Cross-Linked Gelatin/Alginate Hydrogels through Freezing-Drying-Swelling and Freezing-Thawing Processes. *Biomacromolecules* **2024**, *25*, 5758–5770. [CrossRef] [PubMed]
55. Qiao, Y.; Lin, Y.; Zhang, S.; Huang, J. Lanthanide-Containing Photoluminescent Materials: From Hybrid Hydrogel to Inorganic Nanotubes. *Chem. A Eur. J.* **2011**, *17*, 5180–5187. [CrossRef] [PubMed]
56. Huang, C. (Ed.) *Rare Earth Coordination Chemistry: Fundamentals and Applications*, 1st ed.; Wiley: Hoboken, NJ, USA, 2010. [CrossRef]
57. Ma, H.; Shi, Z.; Yang, H.; Yuan, W.; Liang, G.; Zou, J.; Qian, C.; Shen, Z.; Sui, K. Flexible Multicolor-Emitting Lanthanide-Alginate Hybrid Fibers with Multi-Stimuli Responsiveness for Anti-Counterfeiting. *Adv. Compos. Hybrid Mater.* **2024**, *7*, 185. [CrossRef]
58. Budai, L.; Budai, M.; Fülöpné Pápay, Z.E.; Vilimi, Z.; Antal, I. Rheological Considerations of Pharmaceutical Formulations: Focus on Viscoelasticity. *Gels* **2023**, *9*, 469. [CrossRef] [PubMed]
59. El Nokab, M.E.H.; Vojvodin, C.S.; Alghazwat, O.; Zeitoun, E.A.; Vanderveken, M.; Caron, E.; Gautam, I.; Debnath, D.; Husband, B.K.; Hatton, F.L.; et al. Solution Viscosity and Ion-Specific Crosslinking Govern Structure of Alginate and Pectin Hydrogels: Correlating Solid-State NMR with Rheology. *Int. J. Biol. Macromol.* **2026**, *341*, 150321. [CrossRef] [PubMed]
60. Ata, O.; Yazar, G.; Tavman, S.; Kokini, J.L. Linear and Nonlinear Rheological Properties of Gelatin-Chitosan Hydrogels: Evaluation of Crosslinker Concentration and Temperature Effects. *Food Hydrocoll.* **2025**, *163*, 111130. [CrossRef]
61. Huang, Y.; Li, H.; Liu, Z.; Sun, Y.; Chen, X.; Ren, C.; Duan, S.; Nan, G.; Xing, R. The Construction and Characterization of pH-Sensitive Agar/Alginate Hydrogel Beads for Targeted Drug Delivery to the Intestine. *J. Mater. Sci.* **2024**, *59*, 15752–15763. [CrossRef]
62. Manzoor, H.; Arshad, N.; Ur Rehman Qureshi, M.A.; Javed, A. Hydroxyapatite-Reinforced Pectin Hydrogel Films PEC/PVA/APTES/HAp: Doxycycline Loading for Sustained Drug Release and Wound Healing Applications. *RSC Adv.* **2025**, *15*, 30026–30045. [CrossRef] [PubMed]
63. Karaca Açari, İ.; Köytepe, S.; Ateş, B.; Yilmaz, İ.; Seçkin, T. Determination of Characterization, Antibacterial and Drug Release Properties of POSS-Based Film Synthesized with Sol-Gel Technique. *Turk. J. Chem.* **2021**, *45*, 1774–1785. [CrossRef] [PubMed]

64. Turkie, N.S.; Hameed, S.F. A Pioneered Homemade NAG-4SX3-3D Analyzer Coupled with Continuous Flow Injection Analysis New Approach for The On-Line Turbidimetric Measurements of Metronidazole in Pure and Pharmaceutical Formulations. *Chem. Methodol.* **2023**, *7*, 53–66. [CrossRef]
65. Concha, L.; Resende Pires, A.L.; Moraes, A.M.; Mas-Hernández, E.; Berres, S.; Hernandez-Montelongo, J. Cost Function Analysis Applied to Different Kinetic Release Models of Arrabidaea Chica Verlot Extract from Chitosan/Alginate Membranes. *Polymers* **2022**, *14*, 1109. [CrossRef] [PubMed]

Disclaimer/Publisher's Note: The statements, opinions and data contained in all publications are solely those of the individual author(s) and contributor(s) and not of MDPI and/or the editor(s). MDPI and/or the editor(s) disclaim responsibility for any injury to people or property resulting from any ideas, methods, instructions or products referred to in the content.